CHAPTER V
POLYPROPYLENE/POROUS CLAY HETEROSTRUCTURE (PCH) NANOCOMPOSITES

5.1 ABSTRACT

Polypropylene/porous clay heterostructure (PCH) nanocomposites were prepared by melt intercalation method using PP-g-MA as a compatibilizer. The PCH was synthesized by the self-assembly of framework silica around surfactant templates intercalated within the galleries of the smectite clay host. There are two different types of smectite clay were used : montmorillonite (denoted PMH) and bentonite (denoted PBH). The nanocomposites were characterized using XRD, DSC and TG-DTA. Permeability tests of the PP/PCH nanocomposites were also performed. The addition of PMH and PBH does not affect the crystal structure of PP matrix. The melting temperatures of nanocomposites are not different from the pure PP and the crystallization temperatures of nanocomposites are slightly increased. The gas permeability was also investigated.

keywords: porous clay heterostructure, polypropylene, nanocomposites, gas permeability.

5.2 INTRODUCTION

Polypropylene (PP) is one of the most widely used plastics in large volume which is a fast growing thermoplastic that dominates the industrial applications due to its good processibility, great recyclability and low cost. On the other hand, there are many disadvantages of PP, such as low toughness and low service temperature [1]. Recently, the development and characterization of clay mineral-polymer nanocomposites have gained spacial attention because of the advantages in comparison to the traditional polymer composites. The presence of nano-reinforcement of nanoclay (<10 wt%) in nanocomposites can significantly enhance the mechanical, thermal, fire retardancy and barrier performance properties due to the large contact area between polymer and clay on a nanoscale [2].

Up till now, three methods have been suggested for olefin polymers : (1) in situ polymerization, (2) solution method and (3) melt intercalation method. The melt intercalation is the easiest and most cost effective method to prepared nanocomposites [3]. Many studies have examined PP/clay composites prepared using melt intercalation [4,5]

However, Polypropylene (PP) is non-polar or hydrophobic polymer which is not miscible with clay, it is difficult for non-polar PP macromolecules to enter between silicate layers. The presence of a maleic anhydride grafted Polypropylene (PP-g-MA) oligomer can act as compatibilizer. The PP-g-MA oligomer can interact with layers of the clay through strong hydrogen bonding between the polar functional group of PP-g-MA and the oxygen group of silicates. It has been reported that the intercalated PP-g-MA hybrid can be easily dispersed in the polypropylene matrix to form nanocomposites, provided miscible PP-g-MA with the polypropylene [6].

Galarneau who is the first one to prove the possibility of using an intercalated surfactant in combination with the clay interlayer space [7]. These materials are called porous clay heterostructures (PCH). The PCH was prepared by the self-assembly of framework silica around surfactant templates intercalated within the galleries of the smectite clay host. The obtained materials afford the materials with uniform pore diameters in the supermicropore to small mesopore range (1.5 – 3.0 nm).

Many research works have reported on dispersing nanoclay in polypropylene to maximize their physical and mechanical properties. Another material that has an interest is PCH. No research studies about PCH used as a filler in polymer matrix. This makes a great opportunity to study and develop the polymer nanocomposites due to the availability of local clay minerals.

The objective of the present study is to investigate the crystallization behaviors, thermal properties and the permeability of oxygen in polypropylene/PCH films.

5.3 EXPERIMENTAL

Materials

Two different clays have been used in this study for the synthesis of porous clay heterostructures (PCH). Montmorillonite (MMT) was obtained from Kunimine Industries Co., Ltd. and bentonite (BN) was obtained from Thai Nippon Chemical Industry Co., Ltd. which have a cation exchange capacity (CEC) of 115 and 52 mmol/100g clay, respectively.

Alkyltrimethylammonium [$C_nH_{2n+1}N^+(CH_3)_3$] bromide (n = 16) was supplied by A.C.S. Xenon Limited Partnership (Fluka) and chloride (n = 12, 18) were obtained from Kao Industrial (Thailand) Ltd. Tetraehtyl orthosilicate (TEOS) was supplied by A.C.S. Xenon Limited Partnership (Fluka) and dodecylamine was supplied by S.M. Chemical Supplies Co., Ltd.(Aldrich).

Polypropylene (PP), under trademark Moplen HP550R, was obtained from HMC polymers Co., Ltd. Polypropylene grafted maleic anhydride (PP-g-MA), under trademark Polybond®3200 (1 wt% MA graft level), was supplied by Chemtula (Thailand) Ltd.

Synthesis of PCH

3 g of clay was added to 50 mL of alkyltrimethylammonium cation and stirred at 50°C for 24 h. After the exchange reaction the solid was filtrated out, washed with a mixture of methanol and water, and air-dried. The obtained organoclays are named MMT-C_n and BN-C_n (where n is the no. of carbon on the main alkyl chain) for organo-montmorillonite and organo-bentonite. Organoclay was stirred in dodecylamine for 30 min at room temperature after which TEOS was added. The resulting suspension was stirred for further 4 h at room temperature. The molar ratio of organoclay : dodecylamine : TEOS was 1 : 20 : 150. After reaction time the the as-synthesized PCH. was separated by filtration and air-dried overnight at room temperature and calcined at 600°C for 5 h using a temperature ramp rate of 1°C/min. The obtained PCH are named cal-PMH-C_n.

Preparation of Nanocomposites

1 wt% cal-PCH, 3 wt% PP-g-MA and PP were melt blended in a Model T-20 corotating twin-screw extruder (Collin) with L/D=30 and D=25 mm; the processing conditions were the following: temperature (°C): 80, 160, 170, 180, 190, and 200 from hopper to die, respectively and the screw rotation is 50 rpm. Each composition was premixed in a tumble mixer before introducing into the twin-screw extruder to be mixed and extruded through a single strand die, and solidified with cold water and pelletized. The obtained pellet was dried in oven prior to compression molding.

Thin Film Preparation

Thin films were prepared by a Wabash V 50 H 50 ton compression molding machine. The pellets were placed in a mold and the mold was pre-heated at 200°C for 5 minutes without any applied force to allow fully melting. The mold was also compressed at 200°C for a further 5 minutes under a force of 30 tons after that the mold was cooled to 40°C under pressure.

Physical Measurements

X-ray diffraction patterns were measured on a Rigaku Model Dmax 2002 diffractrometer with Ni-filtered Cu K_α radiation operated at 40 kV and 30 mA.

TG-DTA curves were collected on a Perkin-Elmer Pyris Diamond TG/DTA instrument. The sample was loaded on the platinum pan and heated from 30°C to 600°C at a heating rate of 10°C/min under N_2 flow.

DSC analyses were carried out using a Perkin-Elmer DSC 7 instrument. The sample was first heated from 30°C to 250°C and cooled down at a rate of 10°C/min under a N_2 atmosphere with a flow rate of 60 ml/min. The sample was then reheated to 250°C at the same rate.

Scanning electron microscopy was performed on JSM-6400 Model to observe surface morphology of samples. The specimens were coated with gold under vacuum before observation.

Gas permeation experiments were investigated by Brugger Gas Permeability Tester. The sample films were cut into circular shape with 110 mm in diameter according to ASTM 1434-82. The thickness of the films was measured with the

peacock digital thickness gauge model PDN 12N by reading ten points at random position over the entire test area and the results were averaged. The films were placed in a desicator over $CaCl_2$ and kept for not less than 48 h prior to test.

5.4 RESULTS AND DISCUSSION

Characterization of Porous Clay Heterostructures

Montmorillonite (MMT) and bentonite (BN) show a layered or platelike structure in SEM images (Fig. 5.1(A)). The BET surface areas of MMT and BN are 42.07 and 58.52 m^2/g, respectively. This can indicate that MMT and BN are a non-porous solid. The SEM image of porous clay heterostructure after calcination (Fig. 5.1(B)) shows a roughness and a porosity on the surface of clay layers comparing to original montmorillonite.

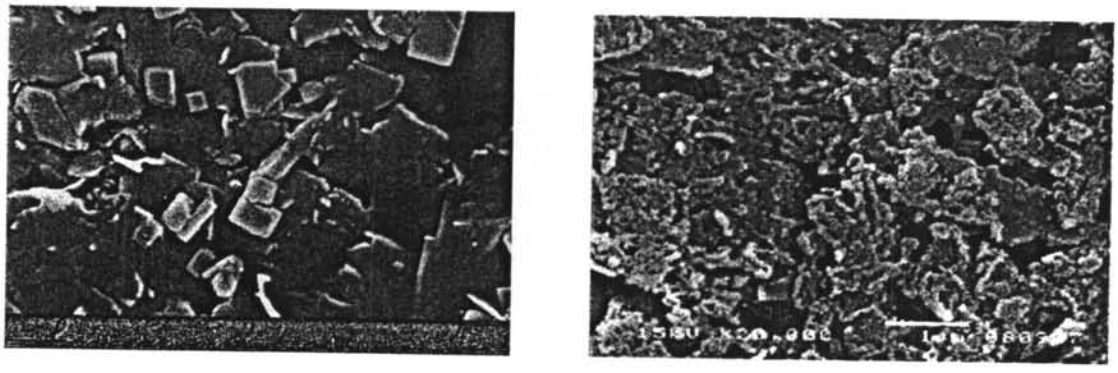

(A) (B)

Figure 5.1 The SEM images: (A) montmorillonite (B) porous clay heterostructure.

The synthesis of PCH can be divided into 2 steps; in the first step the gallery sodium ions in the clay host are exchanged for surfactant ions which are alkyltrimethylammonium cations. The clay layers is expanded, which facilitates the accessibility of co-surfactant (neutral amine) and silica source (TEOS) in the second step. By calcination, the surfactants (templates) are removed from the as-synthesized PMH and PBH. The N_2 adsorption-desorption isotherm of PMH and PBH after calcination are shown in Fig. 5.2, the parameters of which are listed in Table 5.1. The

isotherms of PMH and PBH are similar. The shape of isotherms for both sample has a hysteresis loop which belong to a type IV BET isotherm according to the BDDT classification. The near-linear uptake of nitrogen in the knee region corresponding to the partial pressure range 0.05-0.3 is indicative of a supermicropore to small mesopore structure in the supermicropore to small mesopore region. Furthermore, they exhibit a type B hysteresis loop, indicating the presence of the slit-shaped pores in PMH and PBH [8]. The BET specific surface areas of the calcined PMH and PBH were in the range 500-700 m^2/g and the corresponding pore volumes were in range 0.4-0.5 cm^3/g. The pore sizes which analyzed by BJH method were 1.7-3.8 nm.

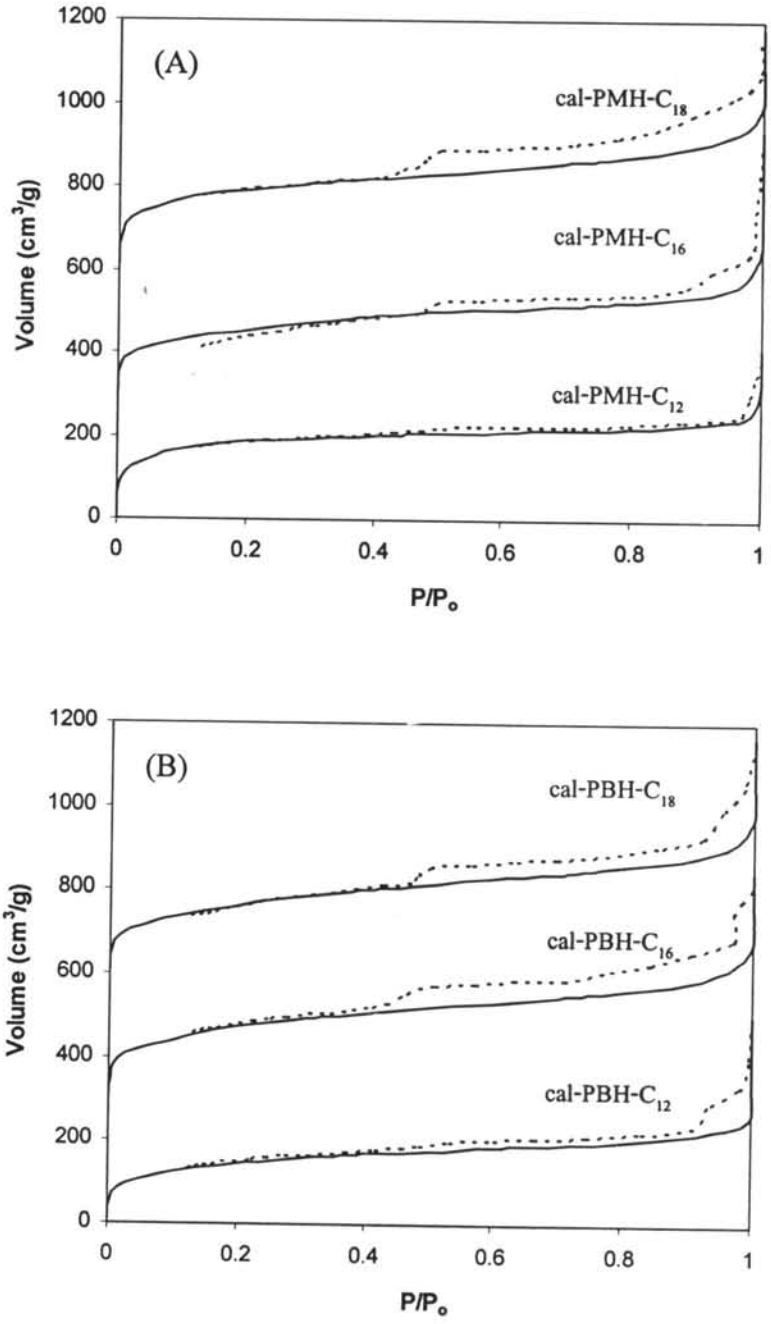

Figure 5.2 The N_2 adroption-desorption isotherm of calcined samples (A) mont-morillonite-PCH (B) bentonite-PCH. Solid line and dash line represent adsorption and desorption, respectively.

Table 5.1 The porosity characteristics of calcined PMH and calcined PBH

Sample	specific surface areas (m^2/g)	Pore specific volume (cm^3/g)	Pore diameter (nm)
cal-PMH-C_{12}	606.57	0.45	1.75
cal-PMH-C_{16}	689.38	0.52	3.88
cal-PMH-C_{18}	746.80	0.51	3.78
cal-PBH-C_{12}	652.90	0.40	2.36
cal-PBH-C_{16}	731.57	0.49	3.71
cal-PBH-C_{18}	729.80	0.47	3.80

Crystal Structure and Crystallinzation Behavior of Nanocomposites

The XRD pattern of PP and nanocomposites are shown in Fig. 5.3 and 5.4. The characteristic peaks of PP α-phase are observed in PP and nanocomposites. Pure PP shows five prominent peaks in the 2θ range of 10-30°, which correspond to monoclinic α crystalline phase : α_1 belongs to the (110) reflection, α_2 to the (040) reflection, α_3 to the (130) reflection and α_4 the (111) and $(\bar{1}31)$(041) reflections [9,10]. The result indicated that there is no observed difference between PP and nanocomposites. The presence of PMH and PBH does not affect the crystal structure of PP matrix in this case.

Fig. 5.6 and 5.8 present the DSC cooling scan thermograms of PP and nanocomposites. The crystallization temperature of PP is 111.11°C, while 3 wt% PP-g-MA addition increase this temperature up to 114.96°C. The addition of PP-g-MA has minimal effect on the crystallization behavior of PP. When the PMH and PBH are added, the crystallization temperatures maintain around 115°C. The addition of PMH and PBH has not much change in this temperature when compared with PP-g-MA/PP. It can be concluded that the change in crystallization temperature is the effect of PP-g-MA in PP matrix.

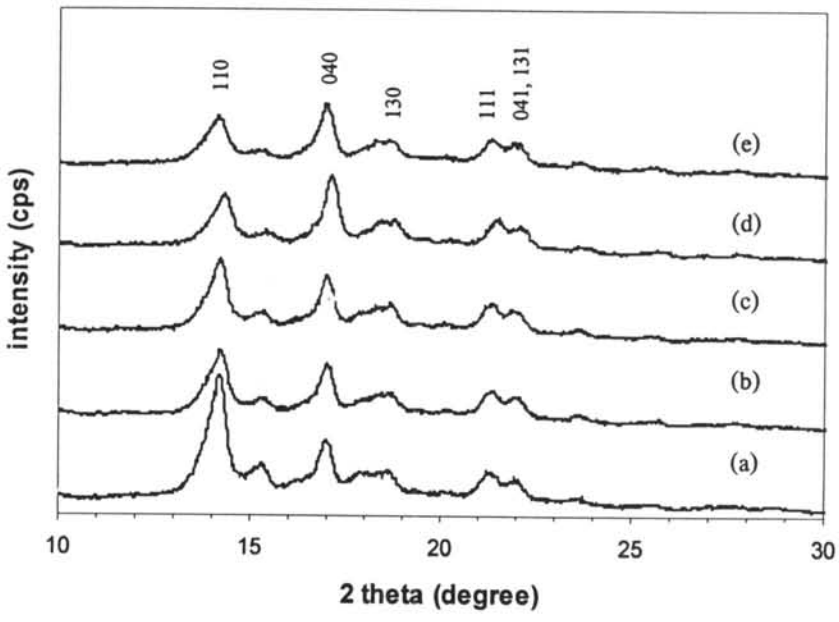

Figure 5.3 The XRD patterns of PMH/PP nanocomposites: (a) pure PP (b) PP-g-MA/PP (c) PMH-C_{12}/PP-g-MA/PP (d) PMH-C_{16}/PP-g-MA/PP (e) PMH-C_{18}/PP-g-MA/PP.

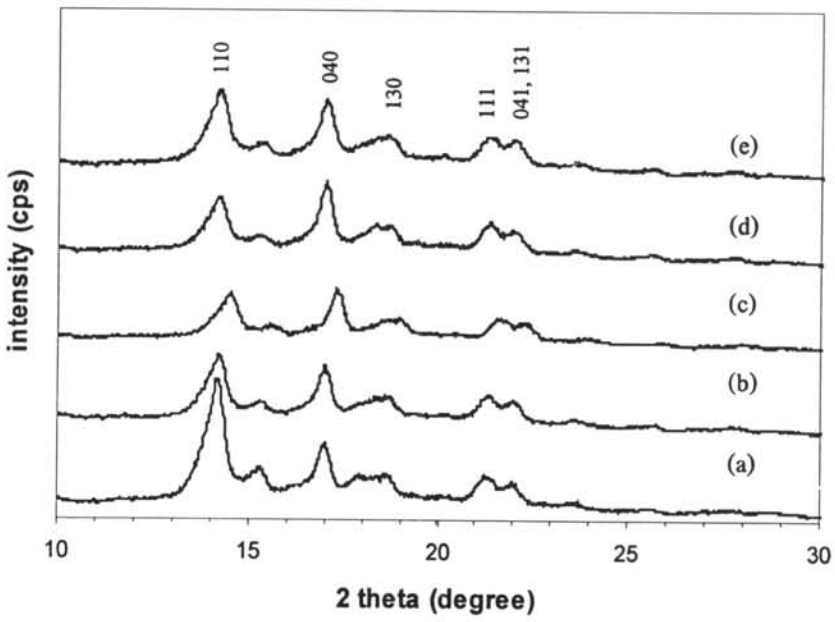

Figure 5.4 The XRD patterns of PBH/PP nanocomposites: (a) pure PP (b) PP-g-MA/PP (c) PBH-C_{12}/PP-g-MA/PP (d) PBH-C_{16}/PP-g-MA/PP (e) PBH-C_{18}/PP-g-MA/PP.

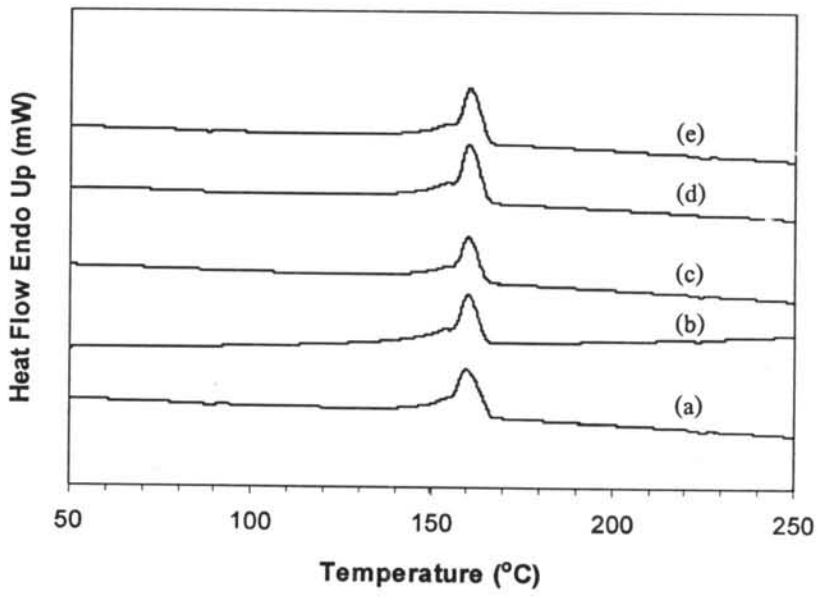

Figure 5.5 DSC heating scan thermograms of (a) pure PP (b) PP-g-MA/PP (c) PMH-C_{12}/PP-g-MA/PP (d) PMH-C_{16}/PP-g-MA/PP (e) PMH-C_{18}/PP-g-MA/PP.

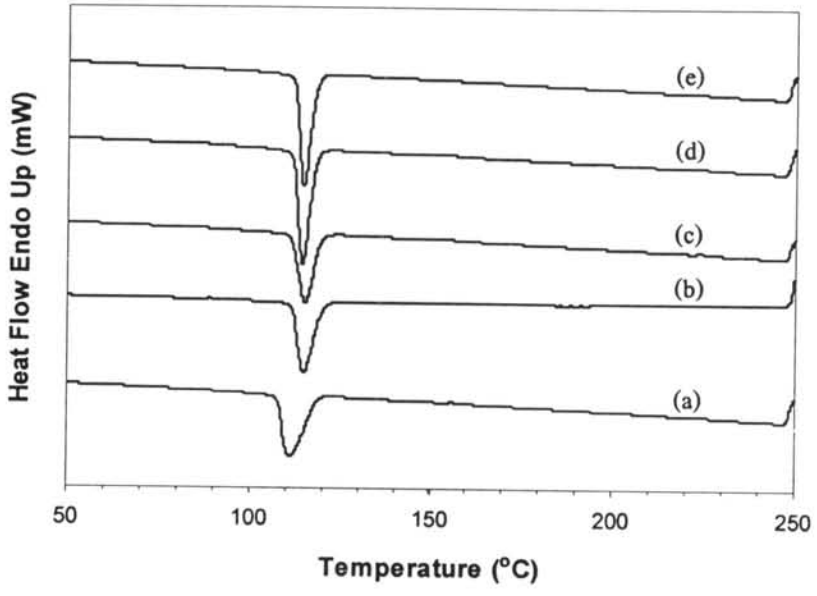

Figure 5.6 DSC cooling scan thermograms of (a) pure PP (b) PP-g-MA/PP (c) PMH-C_{12}/PP-g-MA/PP (d) PMH-C_{16}/PP-g-MA/PP (e) PMH-C_{18}/PP-g-MA/PP.

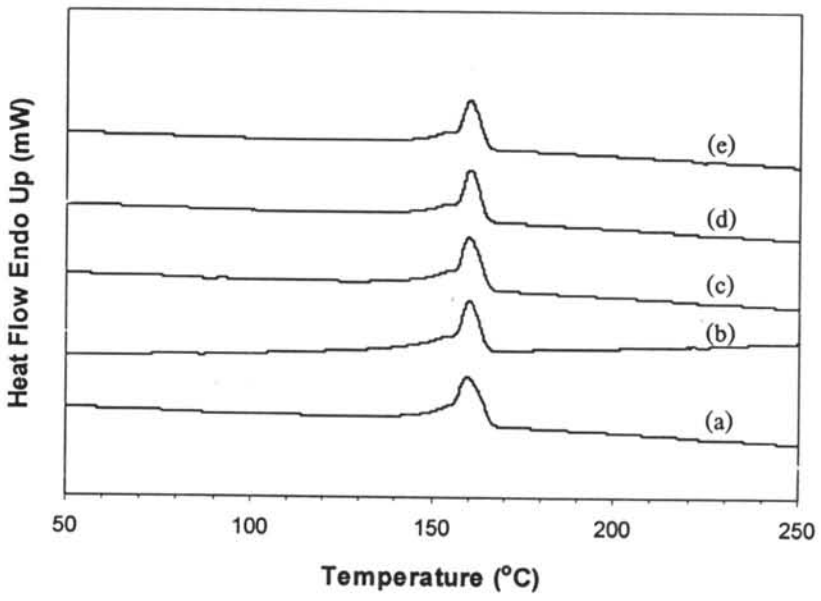

Figure 5.7 DSC heating scan thermograms (a) pure PP (b) PP-g-MA/PP (c) PBH-C_{12}/PP-g-MA/PP (d) PBH-C_{16}/PP-g-MA/PP (e) PBH-C_{18}/PP-g-MA/PP.

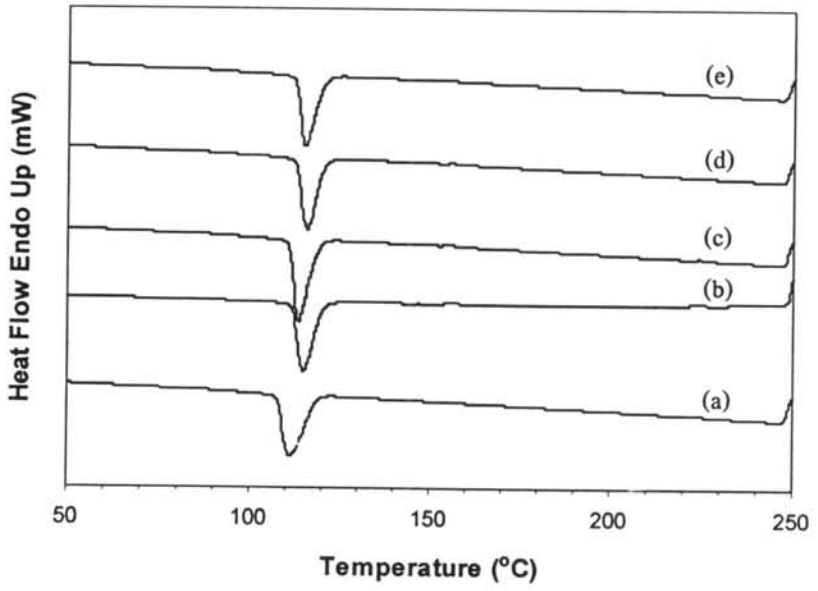

Figure 5.8 DSC cooling scan thermograms (a) pure PP (b) PP-g-MA/PP (c) PBH-C_{12}/PP-g-MA/PP (d) PBH-C_{16}/PP-g-MA/PP (e) PBH-C_{18}/PP-g-MA/PP.

Thermal Properties of Nanocomposites

Fig. 5.5 and 5.7 show the DSC heating scan thermograms of PP and nanocomposites. The melting temperature of PP is 159.53°C and nanocomposites are around 160°C. It seem that the addition of PP-g-MA, PMH and PBH does not change the melting temperature of PP matrix. The TG-DTA curves of PP and nanocomposites are shown in Fig. 5.9 and 5.10 and all results of thermal properties are summarized in Table 5.2. The thermal degradation of PP occurs in one stage from 350 to 500°C. The addition of PP-g-MA could shift the thermal degradation toward higher temperature comparing with pure PP. For the nanocomposites, they show a significant decrease of thermal stability, in term of the degradation temperatures compared to corresponding pure PP and PP-g-MA/PP. Because of porosity, PCH can not act as a mass transport barrier so the volatile product generated during the decomposition can easiliy pass through the pores. It might also be effect on the gas permeability. Another reasons are probably the similar dispersion of this type of clay particles in polymers to the conventional composite, in which the clay particles are still formed tactoid or agglomerated, causing the unimproved thermal stability.

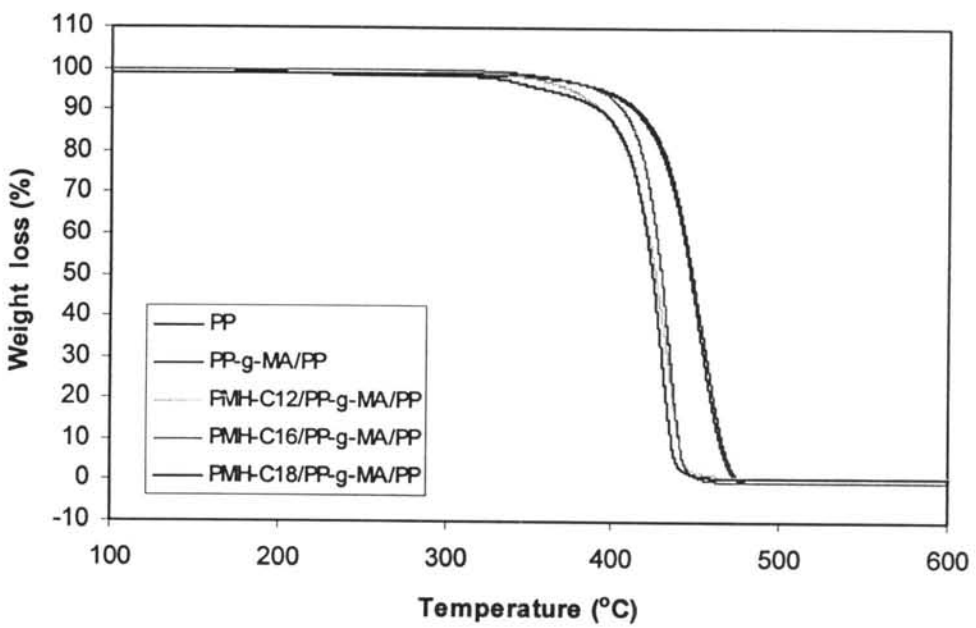

Figure 5.9 TG-DTA curves of pure PP, PP-g-MA/PP and PMH-C_n/PP-g-MA/PP.

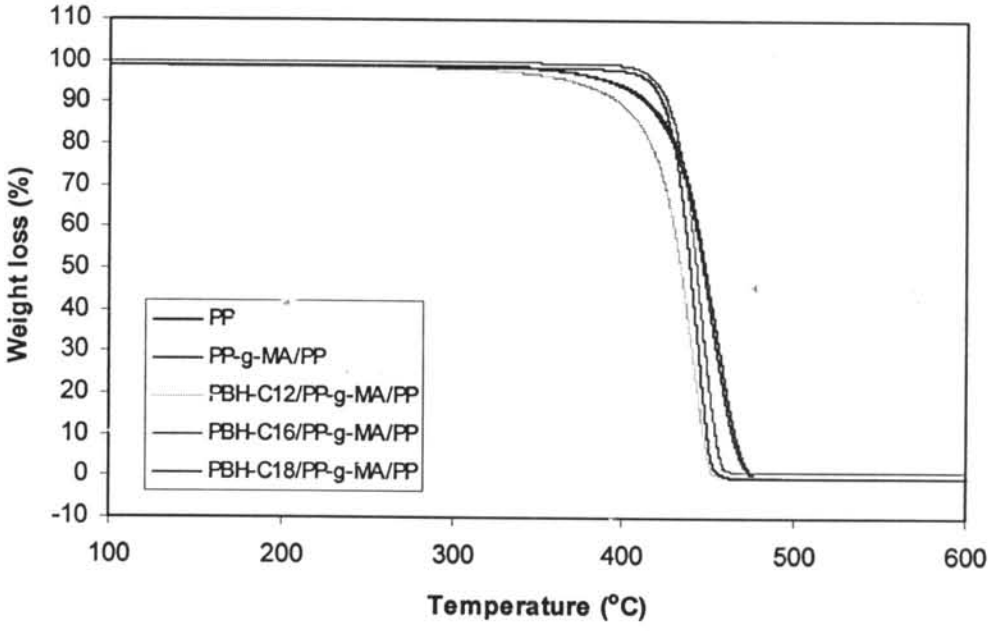

Figure 5.10 TG-DTA curves of pure PP, PP-g-MA/PP and PBH-C_n/PP-g-MA/PP.

Table 5.2 Thermal properties of PP and nanocomposites

Sample	T_m (°C)	T_c (°C)	T_d (°C)	Char residue at 600°C (wt%)
PP	159.53	111.13	453.10	0.5
PP-g-MA/PP	160.03	114.96	457.20	1.4
PMH-C_{12}/PP-g-MA/PP	160.03	115.30	429.20	1.8
PMH-C_{16}/PP-g-MA /PP	160.20	114.46	437.50	1.0
PMH-C_{18}/PP-g-MA /PP	160.36	114.63	432.30	2.0
PBH-C_{12}/PP-g-MA /PP	160.03	113.46	442.80	1.8
PBH-C_{16}/PP-g-MA /PP	160.36	115.63	446.80	1.5
PBH-C_{18}/PP-g-MA /PP	160.20	114.96	446.00	1.1

Gas Permeability

Oxygen transmission rate and permeabilities for PMH and PBH filled PP films are given in table 4.6. The oxygen permeability of PP film is 44.45 $cm^3.mm/m^2.day.atm$ which closes to the reference permeability value. It can be observed that the PMH/PP-g-MA/PP and PBH/PP-g-MA/PP have a higher oxygen transmission rate and permeabitity than pure PP. Generally, the presences of nanoclay (high aspect ratio) in nanocomposites provide the improvement of gas barrier properties due to the hindered diffusion pathways through the nanocomposites [11]. In this case, the addition of fillers may either increase or decrease permeability, depending on their degree of adhesion and compatibility with the polymer. If the polymer and filler are incompatible and lacking adhesion, voids tend to occur at the interface which leads to an increase in free volume of the system and to an increase in gas permeability [12]. Another probable reason is the structure of fillers. Porous clay heterostructures are materials with a combined micro- and mesoporosity which may induce more gas transmission passing through this pore. Due to the incompatibility of PP and PCH, the compatibilizer (PP-g-MA) was added, which may not good enough for giving a strong adhesion between PP and PCH. This approach can result in increasing the oxygen permeability.

Table 5.3 Permeability of PP and nanocomposites

Film sample	Oxygen transmission rate (cm^3/m^2.day.atm)	Oxygen permeability (cm^3.mm/m^2.day.atm)
PP	459.19	44.45
PP-g-MA/PP	476.94	57.76
PMH-C_{12}/PP-g-MA/PP	531.37	54.68
PMH-C_{16}/PP-g-MA /PP	482.17	59.55
PMH-C_{18}/PP-g-MA /PP	535.67	58.66
PBH-C_{12}/PP-g-MA /PP	521.83	49.26
PBH-C_{16}/PP-g-MA /PP	536.32	66.13
PBH-C_{18}/PP-g-MA /PP	531.74	63.86
PP (at 23°C 50% or 0% RH)	-	50-100 [13]

5.5 CONCLUSIONS

Polypropylene/porous clay heterostructure (PCH) nanocomposites were prepared by melt intercalation method using PP-g-MA as a compatibilizer. From the XRD pattern, the five characteristic peaks of PP α-phase are observed in PP amd nanocomposites. The addition of PMH and PBH does not affect the crystal structure of PP matrix. The melting temperatures of nanocomposites are not different from the pure PP and the crystallization temperatures of nanocomposites are slightly increased. It seems that the change in crystallization temperature is the effect of the added PP-g-MA. Thermal stability of nanocomposites tended to decrease because PCH can not act as a mass transport barrier. In addition, the dispersion of this type of clay particles in polymers is formed similar to the conventional composite, in which the clay particles are still formed tactoid or agglomerated, causing unimproved the thermal stability. The oxygen permeability of nanocomposites is higher than pure PP due to the porosity of PCH, which may induce more oxygen transmission passing through.

5.6 ACKNOWLEDGEMENTS

The authors are grateful to Polymer Processing and Polymer Nanomaterials Research Unit. We would like to thank Kunimine Industries Co., Ltd., Thai Nippon Chemical Industry Co., Ltd., Kao Industrial (Thailand) Ltd. and HMC polymers Co., Ltd. for providing the meterials. Finally, we are indebted to Dr. Supapan Seraphin for the collaboration in TEM analysis.

5.7 REFERENCES

[1] Ding, C., Jia, D., He, H., Guo, B., and Hong, H., Polymer Testing 24 (2005) 94.

[2] Arau´jo, E.M., Me´lo, T.J.A., Santana, L.N.L., Neves, G.A., Ferreira, H.C.,Lira, H.L., Carvalho, L.H., A'vila Jr., M.M., Pontes, M.K.G., and Arau´jo, I.S., Materials Science and Engineering B 112 (2004)175.

[3] Sinha Ray, S., and Okamoto, M., Prog. Polym. Sci. 28 (2003) 1539.

[4] Kawasumi, M., Hasegawa, N., Kato, M., Usuki, A., and Okada, A., Macromolecules 30 (1997) 6333.

[5] Ton-That, M.T., Perrin-Sarazin, F., Cole, K.C., Bureau, M.N.,and Denault, J., Polymer Engineering and Science 44 (2004) 1212.

[6] Galgali, G., Ramesh, C., and Lele, A., Macromolecules 34 (2001) 852-858.

[7] Galarneau, A., Barodawalla, A., and Pinnavaia, T.J., Nature 374 (1995) 529.

[8] Gregg, S.J., and Sing, K.S.W., Adsorption, Surface Area and Porosity (second edition), Academic Press, London, (1982) p.116.

[9] Ramos Filho, F.G., Melo, T.A., Rabello, M.S., and Silva, S.M., Polymer Degradation and Stability 89 (2005) 383-392.

[10] Perrin-Sarazin, F., and Ton-That, M.T., Bureau, M.N., and Denault, J., Polymer 46 (2005) 11624-11634.

[11] LeBaron, P.C., Wang, Z., and Pinnavaia, T.J., Applied Clay Science 15 (1999) 11-29.

[12] Wang, Y., Easteal, A.J., and Dong Chen, X., Packag. Technol. Sci. 11 (1998) 169-178.

[13] Lange, J., and Wyser, Y., Packag. Technol. Sci 16 (2003) 149-158.